UNCLASSIFIED: Distribution Statement A. Approved for public release.

Joining of Components of Complex Structures for Improved Dynamic Response

Sung-Kwon Hong[a], Bogdan I. Epureanu[*,a],
Matthew P. Castanier[b]

[a] *Department of Mechanical Engineering, University of Michigan*
2350 Hayward Street, Ann Arbor, Michigan 48109-2125, USA
[b] *U.S. Army Tank Automotive Research,Development, and Engineering Center*
Warren, MI 48397-5000, USA

Abstract

The goal of this work is to provide a method for choosing joining (e.g., bolt) locations for attaching structural reinforcements onto complex structures. The joining locations affect structural performance criteria such as the frequency response and the static compliance of the modified structure. One approach to finding improved/optimal joining locations is to place the joints such that the total amount of energy input into the structure (from external forces) is lowered/minimized, thus ensuring that the performance of the structure is least affected by the structural modifications. However, such an approach does not account for the stresses in the joints. Therefore, in this work, the amount of strain energy concentrated in the joints is also considered. The cost function for this optimization problem is then composed of two energies. These energies are different for the undamped and damped cases. Herein, the focus is on the (more realistic) damped case. The

[*] Corresponding author. Tel.:+1-734-647-6391; fax: +1-734-764-4256
Email addresses: sungkwon@umich.edu (Sung-Kwon Hong), epureanu@umich.edu (Bogdan I. Epureanu), matt.castanier@us.army.mil(Matthew P. Castanier)

Report Documentation Page

Form Approved
OMB No. 0704-0188

Public reporting burden for the collection of information is estimated to average 1 hour per response, including the time for reviewing instructions, searching existing data sources, gathering and maintaining the data needed, and completing and reviewing the collection of information. Send comments regarding this burden estimate or any other aspect of this collection of information, including suggestions for reducing this burden, to Washington Headquarters Services, Directorate for Information Operations and Reports, 1215 Jefferson Davis Highway, Suite 1204, Arlington VA 22202-4302. Respondents should be aware that notwithstanding any other provision of law, no person shall be subject to a penalty for failing to comply with a collection of information if it does not display a currently valid OMB control number.

1. REPORT DATE	2. REPORT TYPE	3. DATES COVERED
03 NOV 2011	**Journal Article**	**03-11-2011 to 03-11-2011**

4. TITLE AND SUBTITLE
JOINING OF COMPONENTS OF COMPLEX STRUCTURES FOR IMPROVED DYNAMIC RESPONSE

5a. CONTRACT NUMBER
w56h2v-04-2-0001

5b. GRANT NUMBER

5c. PROGRAM ELEMENT NUMBER

6. AUTHOR(S)
Matt Castanier; Sung-Kwon Hong; Bogdan Epureanu

5d. PROJECT NUMBER

5e. TASK NUMBER

5f. WORK UNIT NUMBER

7. PERFORMING ORGANIZATION NAME(S) AND ADDRESS(ES)
U.S. Army TARDEC ,6501 E.11 Mile Rd,Warren,MI,48397-5000

8. PERFORMING ORGANIZATION REPORT NUMBER
#22388

9. SPONSORING/MONITORING AGENCY NAME(S) AND ADDRESS(ES)
U.S. Army TARDEC, 6501 E.11 Mile Rd, Warren, MI, 48397-5000

10. SPONSOR/MONITOR'S ACRONYM(S)
TARDEC

11. SPONSOR/MONITOR'S REPORT NUMBER(S)
#22388

12. DISTRIBUTION/AVAILABILITY STATEMENT
Approved for public release; distribution unlimited

13. SUPPLEMENTARY NOTES
submitted to journal of sound an vibration.

14. ABSTRACT

The goal of this work is to provide a method for choosing joining (e.g., bolt) locations for attaching structural reinforcements onto complex structures. The joining locations affect structural performance criteria such as the frequency response and the static compliance of the modified structure. One approach to finding improved/ optimal joining locations is to place the joints such that the total amount of energy input into the structure (from external forces) is lowered/minimized, thus ensuring that the performance of the structure is least affected by the structural modifications. However, such an approach does not account for the stresses in the joints. Therefore, in this work, the amount of strain energy concentrated in the joints is also considered. The cost function for this optimization problem is then composed of two energies. These energies are different for the undamped and damped cases. Herein, the focus is on the (more realistic) damped case. The cost function is minimized by a modified optimality criteria method. This process is time consuming because it requires the calculation of sensitivities of the joint strain energy, which in turn requires the calculation of the displacements of all candidate joint locations by using the system-level mass and stiffness matrices and force vector (at each frequency in the range of interest). To address this issue a series of complex algebraic manipulations and approximations are used to significantly reduce the computational cost. In addition, for the case where structural and geometrical variations are necessary, parametric reduced-order models are used to compute the cost function with further significant gains in computational speed. Numerical results for improved/optimal joining are presented for representative complex structures with structural variabilities.

15. SUBJECT TERMS **joining locations, joint strain energy, parametric reduced-order models**					
16. SECURITY CLASSIFICATION OF:			17. LIMITATION OF ABSTRACT	18. NUMBER OF PAGES	19a. NAME OF RESPONSIBLE PERSON
a. REPORT **unclassified**	b. ABSTRACT **unclassified**	c. THIS PAGE **unclassified**	**Same as Report (SAR)**	**38**	

cost function is minimized by a modified optimality criteria method. This process is time consuming because it requires the calculation of sensitivities of the joint strain energy, which in turn requires the calculation of the displacements of all candidate joint locations by using the system-level mass and stiffness matrices and force vector (at each frequency in the range of interest). To address this issue, a series of complex algebraic manipulations and approximations are used to significantly reduce the computational cost. In addition, for the case where structural and geometrical variations are necessary, parametric reduced-order models are used to compute the cost function with further significant gains in computational speed. Numerical results for improved/optimal joining are presented for representative complex structures with structural variabilities.
Key words: joining locations, joint strain energy, parametric reduced-order models

1. INTRODUCTION

Mechanical structures such as those found in automobiles and airplanes consist of multiple components which are assembled using joints such as bolts, welds, rivets, etc. The locations (assembly points) of these joints affect structural performance characteristics such as the static compliance, the frequency response, and the durability. To achieve high performance, the joining locations should be selected by a systematic approach rather than an experience-based approach. However, this issue can be quite challenging because there are many joints and even more possible joining locations for large scale complex structures. The number of such joints can be as many as several thousand. The choice for joining locations can be improved/optimized by topology optimization approaches such as

homogenization techniques [1] and density methods [2, 3, 4]. Homogenization techniques compute an optimal distribution of micro-structures in a given design domain. Density methods compute an optimal distribution of isotropic materials, where the material densities are design variables. Although the single-component topology design has been extensively studied during the past two decades [5], the amount of research done for multiple-component topology optimization is relatively small. In that area of research, Chirehdast and Jiang [6] extended the concept of topology optimization to the design of spot-weld and adhesive bond patterns. A year later, Jiang and Chirehdast [7] proposed a theoretical framework to determine which optimal connection points minimize the static compliance of the given substructures. To solve the coupled problem of component topology and joining location optimization, Chickermane and Gea [8] considered a methodology for a multiple-component structure as a whole, in which the optimal topology and the joint locations were computed simultaneously. More recently, Zhu and Zhang [9] did layout optimization of structural supports using a topology optimization method for free vibration analyses. All these previous efforts employed spring elements for modeling joints. In contrast, Li et al. [10] proposed a fastener layout/topology that achieves an almost uniform stress level in each joint, and adopted evolutionary structural optimization [11, 12, 13, 14, 15, 16] to provide an alternative optimization strategy to traditional gradient-based topology optimization approaches. In the context of these past efforts, the focus of this work is on the development of an efficient framework for determining improved/optimal joining locations as to minimize the total energy input into the structure and the strain energy in the joints of a complex structure with variability using a density-based method.

For general optimization processes, finite element models (FEMs) are typically used to evaluate the cost function. However, the number of degrees of freedom (DOFs) of FEMs of complex structures are prohibitively large. So, conventional FEMs are hard to employ due to the expensive time needed for each iteration. To reduce the computational cost, Craig-Bampton component mode synthesis (CB-CMS) was employed by Ma et al. [17] in a multi-domain topology optimization. The CB-CMS method is one of the most well-established methods for constructing reduced-order models (ROMs) [18, 19, 20, 21, 22]. However, if one attempts to use CB-CMS techniques when parametric changes (such as thickness and geometrical variations) are applied during the design or exist through damage, the ROMs have to be reconstructed. This reconstruction requires other analyses in addition to the repetitive calculation of the cost function. This is computationally expensive and requires significant effort to prepare a FEM and a ROM for each reanalysis.

These challenges are addressed in this work as follows. First, the mean compliance for the dynamic case with damping is derived, and the strain energy in the joints is added to the cost function. Second, a novel approach to calculate the sensitivity of the strain energy in the joints efficiently is proposed. Third, the cost function and its sensitivity are computed in optimization process by using novel models which are able to manage structural variabilities. Recently, design oriented parametric reduced-order models (PROMs) have been developed to avoid such prohibitively expensive reanalyses of complex structures [23, 24, 25, 26, 27, 28]. Here, the next-generation PROMs (NX-PROMs) [28] developed by the authors are employed to allow complex structures to be divided into several components when determining improved/optimal joining locations.

This paper is organized as follows. In Section 2, a design methodology for determining improved/optimal joining locations is defined, which includes models for the joints, the definition of the associated cost function, and a computationally efficient method to determine design sensitivities for the cost function. In Section 3, NX-PROMs used in the calculations are reviewed. In Section 4, numerical simulations are used to demonstrate the proposed approach for the problem of attaching an armor plate to a structure with a V-shaped bottom. Finally, conclusions are summarized in Section 5

2. DESIGN METHODOLOGY FOR OPTIMAL JOINING LOCATIONS

In single-component topology optimization, the primary objective is to obtain the optimal layout of the structure. When multi-component structures are considered, the problem is extended to select the optimal joining locations between components. This is done not only to optimize the layout of each of the subcomponents, but also because the joining locations affect the structural performance. Herein, a density-based topology optimization technique [2, 3, 4] is applied. Rozvany et al. [29] have defined this method as a modeling technique based on solid isotropic material with penalization (SIMP), where the distribution of the joining stiffness is optimized to improve the static or dynamic structural performance of the entire connected structure. The SIMP method has been developed to replace the size and orientation variables (of the holes used in the homogenization method [1]) with a density variable (of the finite elements) in the design domain. Herein, the idea of SIMP is employed to select optimal joining locations for the entire connected structure. To improve/optimize the joining locations, the stiffnesses of the joints are designed using density functions. Thus, the design vari-

ables are the densities (or stiffnesses) of the joints. These densities are continuous variables varying between 0 and 1. A location where the joint has a low density (close to 0) is not effective/adequate for joining, while a location where the joint has a density close to 1 is best for joining.

2.1. Design Region - Models for Joints

Being one of the controversial tasks in structural FE analysis, modeling methods for joints have been extensively studied. Depending on the required accuracy and complexity of the problem at hand, an appropriate modeling strategy can be adopted for the joints. Several techniques for modeling joints were proposed in the literature [30, 31, 32, 33, 34]. For fatigue analyses based on local stresses and the local strength of the material, a fine mesh of the structure and accurate joint models are required. For noise and vibration analysis of complex structures, a moderate level of accuracy and complexity is required, which leads to simple models for the joints. For a design optimization problem, and especially for a preliminary design, the simple flexible bar models are preferred [6, 8, 32, 35] because those joint models can be easily catered toward the iterative updating employed in design optimization.

In this work, the joints are modeled as three rectilinear springs. Let the stiffness associated with the motion of one of the two ends of a joint (of index i) be $\mathbf{k}_{s,i} = \mathbf{Diag}\left(\begin{bmatrix} k_{x,i} & k_{y,i} & k_{z,i} \end{bmatrix}\right)$, where $k_{x,i}$, $k_{y,i}$, and $k_{z,i}$ denote the stiffnesses of the spring along the three directions of a local Cartesian reference system associated with joint i. Here, $\mathbf{Diag}(\mathbf{v})$ represents a diagonal matrix with entries given by the vector $\mathbf{v}$. The directional stiffnesses of a joint are often related to each other. In this work, it is assumed that $k_{x,i} = k_{z,i} = \alpha_i k_i$ and $k_{y,i} = k_i$. This is the case for joints such as bolts, rivets, spot welds, etc, where y is the axis of the

joint (e.g., the axis of a bolt). Thus, a joint is modeled as having 6 DOFs linked by three springs. The stiffness matrix for the i^{th} joint can thus be written as

$$\mathbf{K}_{s,i} = \begin{bmatrix} \mathbf{k}_{s,i} & -\mathbf{k}_{s,i} \\ -\mathbf{k}_{s,i} & \mathbf{k}_{s,i} \end{bmatrix},$$

where $\mathbf{k}_{s,i} = k_i \mathbf{Diag}\left(\begin{bmatrix} \alpha_i & 1 & \alpha_i \end{bmatrix} \right)$.

The joints (modeled as three rectilinear springs) are designed using density functions in the SIMP method. According to the SIMP method, the design elements are written using the densities ρ_i as

$$\mathbf{K}_{b,i} = \rho_i^p \begin{bmatrix} \mathbf{k}_{s,i} & -\mathbf{k}_{s,i} \\ -\mathbf{k}_{s,i} & \mathbf{k}_{s,i} \end{bmatrix} = \rho_i^p \mathbf{K}_{s,i}, \tag{1}$$

where $\mathbf{K}_{b,i}$ represents the joining stiffness matrix for the i^{th} candidate joining location. Thus, $\mathbf{K}_{b,i}$ is a density-based function. Intermediate values of ρ_i $(0 < \rho_i < 1)$ are penalized compared to values of 0 or 1 by the use of the penalty exponent p. This exponent is typically $p = 3$ for a structural optimization problem [36, 37]. Also, for simplicity, we assume that α_i has the same value for all joints. Thus, only one density variable is assigned to a joint.

The system-level joining stiffness matrix $\mathbf{K}_b$ is given by

$$\mathbf{K}_b = \mathbf{Bdiag} \begin{bmatrix} \mathbf{K}_{b,1} & \mathbf{K}_{b,2} & \cdots & \mathbf{K}_{b,g} \end{bmatrix}, \tag{2}$$

where $\mathbf{Bdiag}$ denotes a block-diagonal matrix, and g is the number of candidate joining locations. Then, the system-level governing equation for the structural dynamic problem with (structural) damping γ is

$$\mathbf{M}_0 \begin{bmatrix} \ddot{\mathbf{u}}_b \\ \ddot{\mathbf{u}}_r \end{bmatrix} + (1 + j\gamma) \left(\mathbf{K}_0 + \begin{bmatrix} \mathbf{K}_b & \mathbf{0} \\ \mathbf{0} & \mathbf{0} \end{bmatrix} \right) \begin{bmatrix} \mathbf{u}_b \\ \mathbf{u}_r \end{bmatrix} = \begin{bmatrix} \mathbf{f}_b \\ \mathbf{f}_r \end{bmatrix}, \tag{3}$$

where $j = \sqrt{-1}$, $\mathbf{M}_0$ and $\mathbf{K}_0$ are the system-level mass and stiffness matrices which do not include the joining stiffness matrix $\mathbf{K}_b$. Subscript b indicates the candidate joining DOFs, and subscript r denotes the remaining DOFs. Note that a joining mass matrix $\mathbf{M}_b$ does not exist because massless spring elements are used. Based on Eq. (3), the dynamic response of all DOFs, $\mathbf{u}_r$ (remainder) and $\mathbf{u}_b$ (joint), are obtained.

2.2. Formulation of the Optimization Problem

The approach employed here is based on an energy criterion which is commonly used in structural optimization problems. Two energies are used. The first is the total energy input into the structure under dynamic loading. This total energy input is equal to the external work done on the structure, which can be defined in function of the mean compliance of the structure. For the dynamic case, the total work done on the structure by external forces is

$$Re\left(\int \mathbf{F}^T d\mathbf{u}\right) = Re\left(\int_0^T \mathbf{F}^{\mathrm{T}} \frac{d\mathbf{u}}{dt} dt\right) = Re\left(\int_0^T \mathbf{F}^{\mathrm{T}} \dot{\mathbf{u}} dt\right), \tag{4}$$

where $\mathbf{F} = \mathbf{f}e^{j\omega t}$ is the external harmonic forcing, and $\mathbf{u}$ is the displacement due to the harmonic forcing. The phase reference for the calculation is chosen such that $\mathbf{f}$ is real. For structures with damping, the response $\mathbf{u}$ is complex and can be expressed as

$$\mathbf{u} = (\mathbf{u}_R + j\mathbf{u}_I)e^{j\omega t} \quad \text{so that} \quad \dot{\mathbf{u}} = (j\omega\mathbf{u}_R - \omega\mathbf{u}_I)e^{j\omega t}, \tag{5}$$

where subscripts R and I indicate real and imaginary parts. From Eq. (5), the real valued portion of the velocity is

$$Re(\dot{\mathbf{u}}) = -\omega\mathbf{u}_I e^{j\omega t} = -\omega\mathbf{u}_I \cos\omega t - \omega\mathbf{u}_R \sin\omega t. \tag{6}$$

Substituting Eq. (6) into Eq. (4) and using the fact that $\mathbf{f}$ is real, one obtains

$$\begin{aligned} Re\left(\int_0^T \mathbf{F}^{\mathrm{T}}\dot{\mathbf{u}}dt\right) &= -\int_0^T \mathbf{f}^{\mathrm{T}}\cos\omega t(\omega\mathbf{u}_I\cos\omega t + \omega\mathbf{u}_R\sin\omega t)dt \\ &= -\omega\mathbf{f}^{\mathrm{T}}\mathbf{u}_I\int_0^T \cos\omega t dt = -\frac{\omega T}{2}\mathbf{f}^{\mathrm{T}}\mathbf{u}_I \\ &= -\pi\mathbf{f}^{\mathrm{T}}\mathbf{u}_I = -\pi(\mathbf{f}^{\mathrm{T}}\mathbf{u})_I. \end{aligned}$$

The resulting first component of the cost function c_1 is thus

$$c_1 = -\left(\mathbf{f}^{\mathrm{T}}\mathbf{u}\right)_I, \tag{7}$$

and contains the strain energy in the entire structure, including the joints. However, focusing on the durability of the joints, the strain energy in the joints should be taken into account. Thus, the second component of the cost function is based on the strain energy in the joints. This energy can be expressed as

$$c_2 = \frac{1}{2}\mathbf{u}_b^{\mathrm{H}}\mathbf{K}_b\mathbf{u}_b, \tag{8}$$

where the superscript H indicates the Hermitian operator. Then, by assembling the two components c_1 and c_2 of the cost function from Eq. (7) and Eq. (8), the final cost function for this optimization problem is

$$c = w_1c_1 + w_2c_2 = -w_1\left(\mathbf{f}^{\mathrm{T}}\mathbf{u}\right)_I + w_2\frac{1}{2}\mathbf{u}_b\mathbf{K}_b^{\mathrm{H}}\mathbf{u}_b,$$

where w_1 and w_2 are weighting factors to control the relative importance of overall structural vibration and joint durability.

Naturally, the number of joints to be distributed in the design domain is limited. Thus, the topology optimization problem associated with the joining location

design can be stated as

$$\begin{aligned} \text{Minimize :} \qquad c(\boldsymbol{\rho}) \;\; &= -w_1 \left(\mathbf{f}^{\mathrm{T}}\mathbf{u}\right)_I + w_2 \frac{1}{2}\mathbf{u}_b \mathbf{K}_b^{\mathrm{T}} \mathbf{u}_b, \\ \text{Subject to :} \qquad g(\boldsymbol{\rho}) \;\; &= \sum_{i=1}^{g} \rho_i - N \leq 0; \;\; 0 < \rho_{min} \leq \rho_i \leq 1, \end{aligned} \tag{9}$$

where N denotes the total number of joints allowed in the design, g is the total number of candidate joint locations, and ρ_{min} is a sufficiently small lower bound imposed to avoid numerical instabilities (herein $\rho_{min} = 0.001$).

To solve such optimization problems, specific methods have been developed to handle a large number of design variables with a few constraints. Among these techniques, the method of moving asymptotes (MMA) [38, 39] and the optimality criterion (OC) [1, 40] methods are broadly utilized for their efficacy and generality. The MMA method is based on the convex approximation method with the advanced feature of setting asymptotic moving limits to approximation variables. The OC makes use of the well-known Karush-Khun-Tucker condition to satisfy a set of criteria related to the behavior of the structure. Even though the OC method is well-convergent for static cases, it is not effective for the dynamic case. Thus, herein we use the modified optimality criterion (MOC) method [40], which is also a gradient-based optimizer.

2.3. Sensitivities of the Cost Function

The design domain for joining is modeled with the density-based three rectilinear springs, each having a design variable ρ_i (density), as in Eq. (1). The variable ρ_i is varied between 0 and 1 using the MOC method to select improved/optimal joining locations. For any gradient-based optimizer, the design sensitivities of the

cost function and of the constraints with respect to the design variables are required. For an efficient calculation of the design sensitivities for the dynamic case discussed here, an adjoint variable method [41] is applied. First, we consider the design sensitivities of c_1 given by in Eq. (7). The derivative of c_1 with respect to the m^{th} design variable ρ_m is

$$\frac{\partial c_1\left(\boldsymbol{\rho}\right)}{\partial \rho_m} = -\left(\begin{bmatrix} \mathbf{f}_b \\ \mathbf{f}_r \end{bmatrix}^T \begin{bmatrix} \frac{\partial \mathbf{u}_b}{\partial \rho_m} \\ \frac{\partial \mathbf{u}_r}{\partial \rho_m} \end{bmatrix} \right)_I = -\left(\begin{bmatrix} \mathbf{f}_b \\ \mathbf{f}_r \end{bmatrix}^T \boldsymbol{\lambda} \right)_I .$$

The direct calculation of $\begin{bmatrix} \frac{\partial \mathbf{u}_b}{\partial \rho_m} \\ \frac{\partial \mathbf{u}_r}{\partial \rho_m} \end{bmatrix}$ is cumbersome, so an adjoint variable $\boldsymbol{\lambda}$ is used. To obtain $\boldsymbol{\lambda}$, the equilibrium Eq. (3) is differentiated with respect to the design variable ρ_m to obtain

$$\frac{\partial \mathbf{G}}{\partial \rho_m} \begin{bmatrix} \mathbf{u}_b \\ \mathbf{u}_r \end{bmatrix} + \mathbf{G} \begin{bmatrix} \frac{\partial \mathbf{u}_b}{\rho_m} \\ \frac{\partial \mathbf{u}_r}{\partial \rho_m} \end{bmatrix} = \mathbf{0}, \tag{10}$$

where

$$\mathbf{G} = -\omega^2 \mathbf{M}_0 + (1 + j\gamma) \left(\mathbf{K}_0 + \begin{bmatrix} \mathbf{K}_b & \mathbf{0} \\ \mathbf{0} & \mathbf{0} \end{bmatrix} \right).$$

Multiplying Eq. (10) by $\begin{bmatrix} \mathbf{u}_b \\ \mathbf{u}_r \end{bmatrix}^{\mathrm{T}}$, one obtains

$$\begin{bmatrix} \mathbf{u}_b \\ \mathbf{u}_r \end{bmatrix}^{\mathrm{T}} \mathbf{G} \begin{bmatrix} \frac{\partial \mathbf{u}_b}{\rho_m} \\ \frac{\partial \mathbf{u}_r}{\partial \rho_m} \end{bmatrix} = \begin{bmatrix} \mathbf{f}_b \\ \mathbf{f}_r \end{bmatrix} \boldsymbol{\lambda} = -\begin{bmatrix} \mathbf{u}_b \\ \mathbf{u}_r \end{bmatrix}^{\mathrm{T}} \begin{bmatrix} \frac{\partial \mathbf{K}_b}{\rho_m} & \mathbf{0} \\ \mathbf{0} & \mathbf{0} \end{bmatrix} \begin{bmatrix} \mathbf{u}_b \\ \mathbf{u}_r \end{bmatrix}.$$

Thus, the design sensitivity of c_1 to ρ_m is given by

$$\begin{aligned}\frac{\partial c_1(\boldsymbol{\rho})}{\partial \rho_m} &= -\left(\begin{bmatrix}\mathbf{f}_b\\ \mathbf{f}_r\end{bmatrix}^{\mathrm{T}}\boldsymbol{\lambda}\right)_I = -\left(\mathbf{u}_b^{\mathrm{T}}\frac{\partial \mathbf{K}_b}{\partial \rho_m}\mathbf{u}_b\right)_I \\ &= -\left(\mathbf{u}_{b,m}^{\mathrm{T}}\frac{\partial\left(\rho_m^p \mathbf{K}_{s,m}\right)}{\partial \rho_m}\mathbf{u}_{b,m}\right)_I = -\left(p\rho_m^{p-1}\mathbf{u}_{b,m}^{\mathrm{T}}\mathbf{K}_{s,m}\mathbf{u}_{b,m}\right)_I.\end{aligned} \tag{11}$$

Second, the sensitivity of c_2 with respect to ρ_m is considered. One obtains

$$\frac{\partial c_2(\boldsymbol{\rho})}{\partial \rho_m} = \frac{1}{2}\left[2\mathbf{u}_b^{\mathrm{H}}\mathbf{K}_b\frac{\partial \mathbf{u}_b}{\partial \rho_m} + \mathbf{u}_b^{\mathrm{H}}\frac{\partial \mathbf{K}_b}{\partial \rho_m}\mathbf{u}_b\right], \tag{12}$$

where the fact that $\mathbf{K}_b$ is a real, symmetric matrix was used. This sensitivity requires the calculation of $\frac{\partial \mathbf{K}_b}{\partial \rho_m}$ and $\frac{\partial \mathbf{u}_b}{\partial \rho_m}$. The first term $\frac{\partial \mathbf{K}_b}{\partial \rho_m}$ can be easily calculated because it has a simple analytical form. Next, from Eq. (10), one obtains

$$\begin{bmatrix}\frac{\partial \mathbf{u}_b}{\partial \rho_m}\\ \frac{\partial \mathbf{u}_b}{\partial \rho_m}\end{bmatrix} = -(1+j\gamma)\,\mathbf{G}^{-1}\begin{bmatrix}\frac{\partial \mathbf{K}_b}{\partial \rho_m}\mathbf{u}_b\\ \mathbf{0}\end{bmatrix}. \tag{13}$$

This equation could, in principle, be used to compute $\frac{\partial \mathbf{u}_b}{\partial \rho_m}$ once $\frac{\partial \mathbf{K}_b}{\partial \rho_m}$ is calculated. However, using Eq. (13) requires the inverse of $\mathbf{G}$ at each iteration. This matrix is very large because it is a full-order, system-level matrix. Also, $\mathbf{G}$ depends on excitation frequency ω, so this inversion has to be done at each frequency in the range of interest. To avoid such a high computational effort, we propose a novel approach. To calculate $\frac{\partial \mathbf{u}_b}{\partial \rho_m}$, first, Eq. (3) is used to obtain

$$\begin{aligned}\left(-\omega^2\mathbf{M}_0 + (1+j\gamma)\,\mathbf{K}_0\right)\begin{bmatrix}\frac{\partial \mathbf{u}_b}{\partial \rho_m}\\ \frac{\partial \mathbf{u}_r}{\partial \rho_m}\end{bmatrix} &+ (1+j\gamma)\begin{bmatrix}\frac{\partial \mathbf{K}_b}{\partial \rho_m} & \mathbf{0}\\ \mathbf{0} & \mathbf{0}\end{bmatrix}\begin{bmatrix}\mathbf{u}_b\\ \mathbf{u}_r\end{bmatrix} \\ &+ (1+j\gamma)\begin{bmatrix}\mathbf{K}_b & \mathbf{0}\\ \mathbf{0} & \mathbf{0}\end{bmatrix}\begin{bmatrix}\frac{\partial \mathbf{u}_b}{\partial \rho_m}\\ \frac{\partial \mathbf{u}_r}{\partial \rho_m}\end{bmatrix} = 0.\end{aligned} \tag{14}$$

Then, substituting Eq. (13) into Eq. (14), one obtains

$$\begin{aligned}\begin{bmatrix} \mathbf{K}_b \frac{\partial \mathbf{u}_b}{\partial \rho_m} \\ \frac{\partial \mathbf{u}_r}{\partial \rho_m} \end{bmatrix} &= \mathbf{G}_0 \mathbf{G}^{-1} \begin{bmatrix} \frac{\partial \mathbf{K}_b}{\partial \rho_m} \mathbf{u}_b \\ \mathbf{0} \end{bmatrix} - \begin{bmatrix} \frac{\partial \mathbf{K}_b}{\partial \rho_m} \mathbf{u}_b \\ \mathbf{0} \end{bmatrix} \\ &= \left(\mathbf{G}_0 \mathbf{G}^{-1} - \mathbf{I} \right) \begin{bmatrix} \frac{\partial \mathbf{K}_b}{\partial \rho_m} \mathbf{u}_b \\ \mathbf{0} \end{bmatrix},\end{aligned} \tag{15}$$

where $\mathbf{G}_0 = \left(-\omega^2 \mathbf{M}_0 + (1 + j\gamma)\, \mathbf{K}_0\right)$. The quantity $\mathbf{G}_0 \mathbf{G}^{-1}$ in Eq. (15) can be written as

$$\mathbf{G}_0 \mathbf{G}^{-1} = \left(\mathbf{I} + (1 + j\gamma) \begin{bmatrix} \mathbf{K}_b & \mathbf{0} \\ \mathbf{0} & \mathbf{0} \end{bmatrix} \mathbf{G}_0^{-1} \right)^{-1}. \tag{16}$$

Then, substituting Eq. (16) into Eq. (15), one obtains

$$\begin{bmatrix} \mathbf{K}_b \frac{\partial \mathbf{u}_b}{\partial \rho_m} \\ \frac{\partial \mathbf{u}_r}{\partial \rho_m} \end{bmatrix} = \left[\left(\mathbf{I} + (1 + j\gamma) \begin{bmatrix} \mathbf{K}_0 & \mathbf{0} \\ \mathbf{0} & \mathbf{0} \end{bmatrix} \mathbf{G}_0^{-1} \right)^{-1} - \mathbf{I} \right] \begin{bmatrix} \frac{\partial \mathbf{K}_b}{\partial \rho_m} \mathbf{u}_b \\ \mathbf{0} \end{bmatrix}. \tag{17}$$

The novel approach uses the assumption that the values of the (spring) stiffnesses of the joints are much smaller than the values of the stiffnesses in the nominal structure. Thus, we assume that, for all DOFs of indices i_1 and i_2,

$$\left(\begin{bmatrix} \mathbf{K}_0 & \mathbf{0} \\ \mathbf{0} & \mathbf{0} \end{bmatrix} \mathbf{G}_0^{-1} \right)_{i_1 i_2} \ll 1.$$

Then, the inverse term in Eq. (17) can be written as

$$\left(\mathbf{I} + (1 + j\gamma) \begin{bmatrix} \mathbf{K}_0 & \mathbf{0} \\ \mathbf{0} & \mathbf{0} \end{bmatrix} \mathbf{G}_0^{-1} \right)^{-1} \approx \mathbf{I} - (1 + j\gamma) \begin{bmatrix} \mathbf{K}_0 & \mathbf{0} \\ \mathbf{0} & \mathbf{0} \end{bmatrix} \mathbf{G}_0^{-1}. \tag{18}$$

Substituting Eq. (18) into Eq. (17), one obtains

$$\begin{bmatrix} \mathbf{K}_b \frac{\partial \mathbf{u}_b}{\partial \rho_m} \\ \frac{\partial \mathbf{u}_r}{\partial \rho_m} \end{bmatrix} = \left(- (1 + j\gamma) \begin{bmatrix} \mathbf{K}_0 & \mathbf{0} \\ \mathbf{0} & \mathbf{0} \end{bmatrix} \mathbf{G}_0^{-1} \right) \begin{bmatrix} \frac{\partial \mathbf{K}_b}{\partial \rho_m} \mathbf{u}_b \\ \mathbf{0} \end{bmatrix}. \tag{19}$$

Of course, Eq. (19) can be used to obtain $\frac{\partial \mathbf{u}_b}{\partial \rho_m}$. However, Eq. (19) requires the calculation of the inverse of $\mathbf{G}_0$. Inverting $\mathbf{G}_0$ has to be done only once during the iterations because $\mathbf{G}_0$ does not depend on $\mathbf{K}_b$. However, $\mathbf{G}_0$ does depend on the excitation frequency ω, which means that $\mathbf{G}_0$ has to be inverted at all frequencies in the range of interest. Also, $\mathbf{G}_0$ is a large matrix because it is a full-order, system-level matrix. Thus, this calculation is very time consuming. A new approach to address this issue is presented next. The key term to be calculated in Eq. (19) is $\mathbf{G}_0^{-1} \begin{bmatrix} \frac{\partial \mathbf{K}_b}{\partial \rho_m}\mathbf{u}_b \\ \mathbf{0} \end{bmatrix}$. To compute this term, we consider first that a unit force is applied at the m^{th} joining location and to the a^{th} DOFs (at that location). The index a varies from 1 to the number L of DOFs used in the finite elements which contain the joining node m. For example, $L = 6$ for shell-type elements, while $L = 3$ for brick-type elements. Then, the resulting deformation $\mathbf{\Psi}_{m,a}$ can be expressed as

$$\mathbf{\Psi}_{m,a} = \mathbf{G}_0^{-1} \cdot \begin{bmatrix} 0 & 0 & \cdots & 1_{m,a} & 0 & 0 \end{bmatrix}^{\mathrm{T}},$$

where $\mathbf{\Psi}_{m,a}$ indicates the deformation everywhere in the system due to the unit force applied at the a^{th} DOFs of the m^{th} joint location.

Next, we express the difficult term as

$$\begin{aligned}
\mathbf{G}_0^{-1}\begin{bmatrix} \frac{\partial \mathbf{K}_b}{\partial \rho_m}\mathbf{u}_b \\ \mathbf{0} \end{bmatrix} &= \sum_{a=1}^{L} \mathbf{G}_0^{-1} \begin{bmatrix} 0 \\ \vdots \\ 1_{m,a} \\ \vdots \\ 0 \end{bmatrix} \left(\frac{\partial \mathbf{K}_{b,m}}{\partial \rho_m}\mathbf{u}_{b,m} \right) \\
&= \sum_{a=1}^{L} \mathbf{\Psi}_{m,a} \frac{\partial \left(\rho_m^p \mathbf{K}_{s,m} \right)}{\partial \rho_m}\mathbf{u}_{b,m} \\
&= \sum_{a=1}^{L} p\rho_m^{p-1} \mathbf{\Psi}_{m,a} \left(\mathbf{K}_{s,m}\mathbf{u}_{b,m} \right)_a .
\end{aligned}$$

Thus, the sensitivity of c_2 in Eq. (12) can be expressed as

$$\frac{\partial c_2\left(\boldsymbol{\rho}\right)}{\partial \rho_m} = \frac{1}{2}\left(-2\sum_{i=1}^{n} \mathbf{A}_i + p\rho_m^{p-1}\mathbf{u}_{b,m}^{\mathrm{H}}\mathbf{K}_{s,m}\mathbf{u}_{b,m} \right), \tag{20}$$

where

$$\mathbf{A}_i = \rho_i^p \mathbf{u}_{b,i}^{\mathrm{H}}\mathbf{K}_{b,i}\left(1+j\gamma\right)\left[\sum_{a=1}^{L} p\rho_m^{p-1}\left(\mathbf{\Psi}_{m,a}\right)_i \left(\mathbf{K}_{s,m}\mathbf{u}_{b,m}\right)_a \right].$$

Finally, the design sensitivity of the entire cost function for the m^{th} design variable is obtained using Eqs. (11) and (20) as

$$\begin{aligned}
\frac{\partial c\left(\boldsymbol{\rho}\right)}{\partial \rho_m} = &- w_1 \left(p\rho_m^{p-1}\mathbf{u}_{b,m}^{\mathrm{T}}\mathbf{K}_s\mathbf{u}_{b,m} \right)_I \\
&+ w_2 \frac{1}{2}\left(-2\sum_{i=1}^{n}\mathbf{A}_i + p\rho_m^{p-1}\mathbf{u}_{b,m}^{\mathrm{H}}\mathbf{K}_s\mathbf{u}_{b,m} \right).
\end{aligned}$$

Computing the sensitivities of the entire cost function based on this formulation is fast especially because vectors $\mathbf{\Psi}_{m,a}$ have to be calculated only once. They remain unchanged during the optimization iterations.

3. PARAMETRIC REDUCED-ORDER MODELS (PROMs)

The cost function and design sensitivities are presented in Section 2 as if they are calculated based on full-order finite element models. However, if the structure has a huge number of DOFs, the turn-around time of the optimization iteration process is very long. This issue is particularly important when the design involves not only choosing joining locations, but also modifications of various components of the structure. In that case, the full-order model of the modified components changes, which requires additional computational effort. To address this issue, a new modeling approach is presented next. This approach is based on next-generation parametric reduced-order models (NX-PROMs) [28] used together with the well-known fixed-interface Craig-Bampton component mode synthesis (CB-CMS) [19]. A review of this approach is provided next.

3.1. Modeling Approach

CB-CMS [19] is used to model only the substructures which do not have any structural variability. This modeling approach is used because it is very simple and computationally stable. To apply CB-CMS, the complex structure of interest is divided into several substructures, and their DOFs are partitioned into internal and interface DOFs. The interface DOFs for a substructure (of index q) are projected onto the generalized coordinates by using static constraint modes $\mathbf{\Psi}_q^C$. The internal DOFs are projected onto fixed-interface normal modes $\mathbf{\Phi}_q^N$. Then, the size of the mass and stiffness matrices and the force vector for substructure q is significantly reduced as follows

$$\mathbf{M}_q^{CB} = \begin{bmatrix} \mathbf{m}_q^C & \mathbf{m}_q^{CN} \\ \mathbf{m}_q^{NC} & \mathbf{m}_q^N \end{bmatrix}, \mathbf{K}_q^{CB} = \begin{bmatrix} \mathbf{k}_q^C & \mathbf{k}_q^{CN} \\ \mathbf{k}_q^{NC} & \mathbf{k}_q^N \end{bmatrix}, \mathbf{F}_q^{CB} = \begin{bmatrix} \mathbf{f}_q^C \\ \mathbf{f}_q^N \end{bmatrix},$$

where the superscript C indicates generalized interface DOFs (i.e., constraint partitions). These DOFs are used to assemble substructural matrices and obtain system-level reduced matrices. The superscript N indicates generalized internal DOFs. These DOFs are used to reduce the number of internal DOFs.

The substructures which can have variability are modeled using NX-PROMs [28]. One important advantage of NX-PROMs is that the finite element mesh of the nominal structure does not need to be modified although several substructures may have variability. That is because the mass and stiffness matrices of these substructures are parameterized. The NX-PROM approach resembles the CB-CMS approach. However, the transformation matrix for NX-PROMs is constructed for all values of the variable parameters in the parameter space of each component with variability. In contrast, components with no parameter variability do not need a parameterization, so they are modeled by CB-CMS. By applying the NX-PROM approach to the l^{th} substructure with variation Δp in one of its parameters, the mass and stiffness matrices and force vector are obtained as

$$\begin{aligned}
\mathbf{M}_l^{NX} &= \begin{bmatrix} \mathbf{m}_{\Delta p,l}^{C} & \mathbf{m}_{\Delta p,l}^{CN} \\ \mathbf{m}_{\Delta p,l}^{NC} & \mathbf{m}_{\Delta p,l}^{N} \end{bmatrix}, \mathbf{K}_l^{NX} = \begin{bmatrix} \mathbf{k}_{\Delta p,l}^{C} & \mathbf{k}_{\Delta p,l}^{CN} \\ \mathbf{k}_{\Delta p,l}^{NC} & \mathbf{k}_{\Delta p,l}^{N} \end{bmatrix}, \\
\mathbf{F}_l^{NX} &= \begin{bmatrix} \mathbf{f}_{\Delta p,l}^{C} \\ \mathbf{f}_{\Delta p,l}^{N} \end{bmatrix},
\end{aligned}$$

3.2. Geometric Compatibility Conditions

The complete, reduced-order component-level equations of motion for each component l of the entire set of n components can be expressed as

$$\mathbf{M}_l^{ROM}\ddot{\mathbf{q}}_l^{ROM} + \mathbf{K}_l^{ROM}\mathbf{q}_l^{ROM} = \mathbf{F}_l^{ROM}, \tag{21}$$

where the superscript ROM indicates that either CB-CMS or NX-PROM was used, with q_l being the generalized coordinates ($l = 1, \cdots, n$).

The constraint partitions (indicated by superscript C) of component-level matrices retain the physical meaning of the interface DOFs. This means that the geometric compatibility conditions at the interfaces with no joints can be applied directly to construct the system-level matrices. Consider, for example that an interface with no joints exists between components l and d ($d = 1, \cdots, n$, $d \neq l$). Then,

$$\mathbf{q}_l^C = \mathbf{q}_d^C, \tag{22}$$

where $\mathbf{q}_l^C$ and $\mathbf{q}_d^C$ are the generalized coordinates for the constraint partitions that correspond to the interface between substructures l and d. Of course, there is no compatibility condition to be enforced for two components which do not have a common interface. Equation (22) is used to transform the matrices in Eq. (21) in a manner similar to the assembly process in all finite element modeling methods. Then, the system-level equation of motion which does not include the joints is given by

$$\mathbf{M}_{sys}^{ROM}\ddot{\mathbf{q}}_{sys}^{ROM} + \mathbf{K}_{sys}^{ROM}\mathbf{q}_{sys}^{ROM} = \mathbf{F}_{sys}^{ROM}. \tag{23}$$

Equation (23) is obtained after all geometric compatibility condition have been enforced, except for the conditions present at the interfaces with joints. To tackle the joints, the (remaining) constraint partitions corresponding to the joints are repartitioned in two pieces. These pieces are indicated by superscript C_1 and C_2. The C_1 portion corresponds the DOFs of one end of all joints and the C_2 portion corresponds to the DOFs of the other end of all joints. Thus, the matrices in

Eq. (23) can be expressed as

$$\begin{aligned}
\mathbf{M}_{sys}^{ROM} &= \begin{bmatrix} \mathbf{M}^{\bar{C}} & \mathbf{M}^{\bar{C}N} \\ \mathbf{M}^{N\bar{C}} & \mathbf{M}^{N} \end{bmatrix} = \begin{bmatrix} \mathbf{M}^{C_1} & \mathbf{0} & \mathbf{M}^{C_1N} \\ \mathbf{0} & \mathbf{M}^{C_2} & \mathbf{M}^{C_2N} \\ \mathbf{M}^{NC_1} & \mathbf{M}^{NC_2} & \mathbf{M}^{N} \end{bmatrix}, \\
\mathbf{K}_{sys}^{ROM} &= \begin{bmatrix} \mathbf{K}^{\bar{C}} & \mathbf{K}^{\bar{C}N} \\ \mathbf{K}^{N\bar{C}} & \mathbf{K}^{N} \end{bmatrix} = \begin{bmatrix} \mathbf{K}^{C_1} & \mathbf{0} & \mathbf{K}^{C_1N} \\ \mathbf{0} & \mathbf{K}^{C_2} & \mathbf{K}^{C_2N} \\ \mathbf{K}^{NC_1} & \mathbf{K}^{NC_2} & \mathbf{K}^{N} \end{bmatrix}, \\
\mathbf{q}_{sys}^{ROM} &= \begin{bmatrix} \mathbf{q}^{\bar{C}} \\ \mathbf{q}^{N} \end{bmatrix} = \begin{bmatrix} \mathbf{q}^{C_1} \\ \mathbf{q}^{C_2} \\ \mathbf{q}^{N} \end{bmatrix}, \quad \mathbf{F}_{sys}^{ROM} = \begin{bmatrix} \mathbf{F}^{\bar{C}} \\ \mathbf{F}^{N} \end{bmatrix} = \begin{bmatrix} \mathbf{F}^{C_1} \\ \mathbf{F}^{C_2} \\ \mathbf{F}^{N} \end{bmatrix},
\end{aligned} \tag{24}$$

where superscript $\bar{C}$ represents the constraint partition (for all components) that corresponds to the joints.

Next, the joints (three rectilinear springs) are applied to connect the DOFs of C_1 to those of C_2. First, the joining stiffness matrix in Eq. (2) and the physical coordinates of all DOFs of all joints are partitioned similar to C_1 and C_2 to obtain

$$\mathbf{K}_b = \begin{bmatrix} \mathbf{K}_b^{C_1} & \mathbf{K}_b^{C_1C_2} \\ \mathbf{K}_b^{C_2C_1} & \mathbf{K}_b^{C_2} \end{bmatrix} \text{ and } \mathbf{q}_b = \begin{bmatrix} \mathbf{q}_b^{C_1} \\ \mathbf{q}_b^{C_2} \end{bmatrix}. \tag{25}$$

The C_1 and C_2 partitions are the same in Eqs. (24) and (25). Thus,

$$\mathbf{q}^{C_1} = \mathbf{q}_b^{C_1} \text{ and } \mathbf{q}^{C_2} = \mathbf{q}_b^{C_2}. \tag{26}$$

Ultimately, Eq. (26) is used to obtain the final system-level equation of motion *with joints* expressed as

$$\hat{\mathbf{M}}_{sys}^{ROM}\ddot{\mathbf{q}}_{sys}^{ROM} + \hat{\mathbf{K}}_{sys}^{ROM}\mathbf{q}_{sys}^{ROM} = \hat{\mathbf{F}}_{sys}^{ROM}, \tag{27}$$

where

$$\hat{\mathbf{M}}_{sys} = \mathbf{M}_{sys},\ \hat{\mathbf{K}}_{sys} = \begin{bmatrix} \mathbf{K}^{C_1} + \mathbf{K}_b^{C_1} & \mathbf{K}_b^{C_1C_2} & \mathbf{K}^{C_1N} \\ \mathbf{K}_b^{C_2C_1} & \mathbf{K}^{C_2} + \mathbf{K}_b^{C_2} & \mathbf{K}^{C_2N} \\ \mathbf{K}^{NC_1} & \mathbf{K}^{NC_2} & \mathbf{K}^{N} \end{bmatrix} \text{ and}$$

$$\hat{\mathbf{F}}_{sys} = \mathbf{F}_{sys}.$$

Note that all the design parameters are contained in the joints. Thus, the joining optimization has to reevaluate only the joints, and does not require a reevaluation of all components. Moreover, all components (except for the joints) are reduced only once, at the initial construction of NX-PROMs, before iteration. Thus, the joining design can be very efficient by using NX-PROMs with the proper matrix partitioning. By using the system matrices in Eq. (27) (based on NX-PROMs), the turn-around time of the iteration process is much shorter than by using FEMs. Additionally, variations in any substructure (where NX-PROM is used) can be handled efficiently in the new optimization processes.

4. NUMERICAL EXAMPLE: V-SHAPED BOX STRUCTURE WITH THICKNESS VARIATIONS

To demonstrate the improved/optimal joining, a structure with a V-shaped bottom is considered, as shown in Figure 1. The focus of this example is to find joining locations where to attach an armor plate to the structure. Figure 1 shows all substructures and their number. The marked regions are candidate joining locations. Harmonic loads are assumed to act on substructure 5 shown in Figure 3. Substructure 6 and the armor plate have thickness variations. Table 1 shows two cases of thickness variation of each substructure. NX-PROMs are constructed by parameterizing the thickness of substructure 6 and of the armor plate. CB-CMS

is applied to all remaining substructures because they do not have structural variations.

As an initial guess, all the candidate joining nodes on substructure 4 and on the armor plate are connected by three rectilinear springs as shown in Figure 2. For all joints, the maximum allowable stiffness of the spring in the (main) y direction is $k_y = k_0 = 500\ kN/m$, and the other directional stiffnesses are $k_x = k_z = 0.5\ k_0$. The total number of candidate joints is 54, and the final desired number of joints g is 10 or 11. Note that the four edge nodes highlighted in Figure 2 are not considered candidate joining locations. The fact that joints are present at those four locations is considered to be known.

The optimization starts with an initial guess, i.e. a given set of feasible design values ($\rho_i = 0.185$ when $N = 10$, and $\rho_i = 0.204$ when $N = 11$). The structural damping is $\gamma = 0.03$, and the weighting factors in Eq. (9) are $w_1 = 0.5$ and $w_2 = 0.5$. With the given initial guess, the excitation frequency was fixed at $30\ Hz$ for the nominal structure. Figure 4 shows the results of the optimization for the $30\ Hz$ excitation and $N = 10$. Figures 5, 6 and 7 show the results of the optimization for a $100\ Hz$ excitation for the nominal structure and for cases 1 and 2 of thickness variations. For the nominal structure under the $100\ Hz$ excitation, $N = 11$. For cases 1 and 2 of thickness variation, $N = 10$.

The optimal joining locations described in Figure 5 are selected differently for each case, even though the thickness variations are not very large. However, the cost function is minimized for all 3 cases, as shown in Figure 6. Figure 7 shows the changes in natural frequencies at each iteration. Note that the various choices made during the iterations affect significantly the dynamic response because some of the natural frequencies of the overall structure change significantly.

5. CONCLUSIONS

Several challenges of current methods for determining improved/optimal joining locations have been addressed. First, the mean compliance for the dynamic case with damping was derived, and the strain energy in the joints was added to the cost function. Second, a novel approach to calculate efficiently the sensitivity of the strain energy in the joints was proposed. Third, the cost function and its sensitivities were computed in the optimization process by using novel next-generation parametric reduced-order models to improve computational efficiency and to manage structural variabilities in several substructures.

The approach to select improved/optimal joining locations uses a density-based topology optimization method which employs solid isotropic material with penalization (SIMP) modeling. Based on SIMP modeling, a three rectilinear springs (with density) is used to model each joint. Also, a reliable cost function has been developed. It includes the energy input into the structure and the strain energy in all joints. By penalizing the density of the springs between 0 and 1, the cost function is minimized while satisfying a constraint which enforces an upper limit for the number of joints in the design domain. To solve this optimization problem, the modified optimality criterion method has been applied. To demonstrate the methodology, the problem of attaching armor to a structure with a V-shaped bottom has been considered. By applying the proposed methodology, improved/optimal joining locations have been selected.

Acknowledgment

The authors gratefully acknowledge the financial support of the Automotive Research Center, a U.S. Army Center of Excellence for Modeling and Simulation

of Ground Vehicles led by the University of Michigan.

Reference herein to any specific commercial company, product, process, or service by trade name, trademark, manufacturer, or otherwise, does not necessarily constitute or imply its endorsement, recommendation, or favoring by the United States Government or the Department of the Army (DoA). The opinions of the authors expressed herein do not necessarily state or reflect those of the United States Government or the DoA, and shall not be used for advertising or product endorsement purposes.
UNCLASSIFIED: Dist A. Approved for public release.

References

[1] M. P. Bendsøe, N. Kikuchi, Generating optimal topologies in structural design using a homogenization method, Computer Methods in Applied Mechanics and Engineering 71 (1988) 197–224.

[2] M. P. Bendsøe, Optimal shape design as a material distribution problem, Structural Optimization 1 (1989) 193–202.

[3] M. Zhou, G. I. N. Rozvany, The COC algorithm, Part II: Topological, geometrical and generalized shape optimization, Computer Methods in Applied Mechanics and Engineering 89 (1991) 309–336.

[4] R. J. Yang, A. I. Chahande, Automotive applications of topology optimization, Structural Optimization 9 (1995) 246–249.

[5] M. P. Bendsøe, O. Sigmund, Topology Optimization: Theory, Methods and Applications, Springer, 2002.

[6] M. Chirehdast, T. Jiang, Optimal design of spot-weld and adhesive bond patterns, in: Proceedings of the International Congress and Exposition SAE, Paper No. 960812, 1996.

[7] T. Jiang, M. Chirehdast, A system approach to structural topology optimization: Designing optimal connections, ASME Transations: Journal of Mechanical Design 119 (1997) 40–47.

[8] H. Chickermane, H. C. Gea, Design of multi-component structural systems for optimal layout topology and joint locations, Engineering with Computers 13 (1997) 235–243.

[9] J. H. Zhu, W. H. Zhang, Maximization of structural natural frequency with optimal support layout, Structural and Multidisciplinary Optimization 31(6) (2006) 462–469.

[10] Q. Li, G. P. Steven, Y. Xie, Evolutionary structural optimization for connection topology design of multi-component systems, Engineering Computations 18(3-4) (2001) 460–479.

[11] Y. M. Xie, G. P. Steven, A simple evolutionary procedure for structural optimization, Computer and Structures 49 (1993) 885–896.

[12] Y. M. Xie, G. P. Steven, Optimal design of multiple load case structures using an evolutionary procedure, Engineering Computations 11 (1994) 295–302.

[13] Y. M. Xie, G. P. Steven, Evolutionary Structural Optimization, Springer-Verlag, 1997.

[14] E. Hinton, J. Sienz, Fully stressed topological design of structure using an evolutionary procedure, Engineering Computations 12 (1995) 229–244.

[15] E. Hinton, J. Sienz, S. Bulman, S. J. Lee, Fully integrated design optimization of engineering structures using adaptive finite element models, in: Proceedings of the Australasian Conference no Structural Optimization, 2011, pp. 73–78.

[16] P. Roski, Three-dimensional topology design of structures using crystal models, Computer and Structures 55 (1995) 1077–1083.

[17] Z. D. Ma, N. Kikuchi, C. Pierre, B. Raju, Multi-domain topology optimization for vehicle substructure design, in: Proceedings of ASME IMECE, 2002, pp. 2002–32908.

[18] W. C. Hurty, Dynamic analysis of structural systems using component modes, AIAA Journal 3 (4) (1965) 678–685.

[19] R. R. Craig, M. C. C. Bampton, Coupling of substructures for dynamic analyses, AIAA Journal 6 (7) (1968) 1313–1319.

[20] S. Rubin, Improved component-mode representation for structural dynamic analysis, AIAA Journal 13 (8) (1975) 995–1006.

[21] R. M. Hintz, Analytical methods in component mode synthesis, AIAA Journal 13 (8) (1975) 1007–1016.

[22] R. R. Craig, Jr., C.-J. Chang, Free-interface methods of substructure coupling for dynamic analysis, AIAA Journal 14 (11) (1976) 1633–1635.

[23] E. Balmès, Parametric families of reduced finite element modes: Theory and application., Mechanical Systems and Signal Processing 10 (4) (1996) 381–394.

[24] E. Balmès, F. Ravary, D. Langlais, Uncertainty propagation in modal analysis, in: Proceedings of IMAC-XXII: A Conference and Exposition on Structural Dynamics, 2004, pp. 57.

[25] G. Zhang, M. P. Castanier, C. Pierre, Integration of component-based and parametric reduced-order modeling methods for probabilistic vibration analysis and design., in: Proceedings of the European Conference on Structural Dynamics, 2005, pp. 993–998.

[26] K. Park, Component-based vibration modeling methods for fast reanalyses and design of complex structures, Ph.D. Thesis, University of Michigan (2008).

[27] S.-K. Hong, B. I. Epureanu, M. P. Castanier, D. J. Gorsich, Parametric reduced-order models for predicting the vibration response of complex structures with component damage and uncertainties., Journal of Sound and Vibration 330 (2011) 1091–1110.

[28] S.-K. Hong, B. I. Epureanu, M. P. Castanier, Next-generation parametric reduced-order models, Computer Method for Applied Mechanics and Engineering, submitted.

[29] G. I. N. Rozvany, M. Zhou, T. Birker, Generalized shape optimization without homogenization, Structural Optimization 4 (1992) 250–252.

[30] D. Heiserer, M. Chargin, J. Sielaff, High performance, process oriented, weld spot approach, in: Proceedings of MSC Worldwide Automotive, 1999.

[31] J. Fang, C. Hoff, B. Holman, F. Mueller, D. Wallerstein, Welding modeling in MSC Nastran, in: Proceedings MSC Worldwide Automotive, 2000.

[32] Y. Zhang, D. Taylor, Optimization of spot-welded structures, Finite Elements in Analysis and Design 37 (9) (2001) 1013–1022.

[33] M. Palmonella, M. I. Friswell, J. E. Mottershead, L. A. W., Guidelines for the implementation of the CWELD and ACM2 Spot Weld Models in Structural Dynamics, Finite Elements in Analysis and Design 41 (2004) 193–210.

[34] S. Donders, M. Brughmans, The effect of spot weld failure on dynamic vehicle performance, Sound and Vibration 39 (4) (2005) 16–25.

[35] S. W. Chae, K. Y. Kwon, L. T. S., An optimal design system for spot welding locations, Finite Elements in Analysis and Design 38 (2002) 276–294.

[36] M. P. Bendsøe, O. Sigmund, Material interpolation schemes in topology optimization, Archive of Applied Mechanics 69 (1999) 635–654.

[37] O. Sigmund, A 99 line topology optimization code written in matlab, Structural dna Multidisciplinary Optimization 21 (2) (2001) 120–127.

[38] K. Svanberg, The method of moving asymptotes - a new method for structural optimization, International Journal for Numerical Methods in Engineering 24 (1987) 359–373.

[39] K. Svanberg, A class of globally convergent optimization methods based on conservative convec separable approximations, SIAM Journal on Optimization 12 (2) (2002) 555–573.

[40] Z. D. Ma, N. Kikuchi, I. Hagiwara, Structural topology and shape optimization for a frequency response problem, Computational Mechanics 13 (1993) 157–174.

[41] K. K. Choi, N. H. Kim, Structural Sensitivity Analysis and Optimization I: Linear Systems, Springer, 2005.

List of Tables

1 Thickness variations for substructure 5 and for the armor plate . . 30

Table 1: Thickness variations for substructure 5 and for the armor plate

Substructure	Nominal	Case 1	Case 2
6	6 *mm*	7.5 *mm*	8.5 *mm*
Armor plate	10 *mm*	10.5 *mm*	11.1 *mm*

List of Figures

1 Structure with a V-shaped bottom; indices of the substructures are shown 32

2 Springs modeling joints between substructure 4 and the armor plate 33

3 Dynamic loads applied to substructure 5 to excite symmetric and asymmetric modes of the entire structure 34

4 (a) 10 optimal joining locations, (b) convergence history, and (c) natural frequency variations for a 30 *Hz* excitation of the nominal structure 35

5 Optimal joining locations for a 100 *Hz* excitation for (a) nominal structure, (b) case 1 (c) case 2 of thickness variation 36

6 Convergence history for a 100 *Hz* excitation for (a) nominal structure, (b) case 1 (c) case 2 of thickness variation 37

7 Natural frequency variation for a 100 *Hz* excitation for (a) nominal structure, (b) case 1 (c) case 2 of thickness variation 38

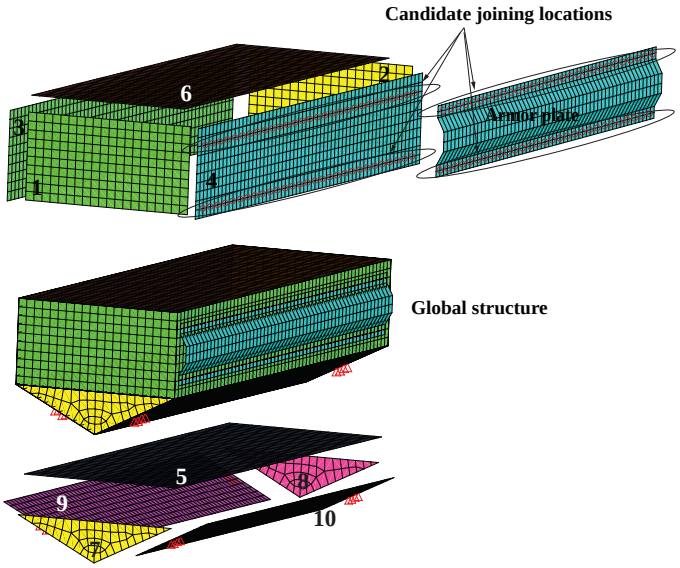

Figure 1: Structure with a V-shaped bottom; indices of the substructures are shown

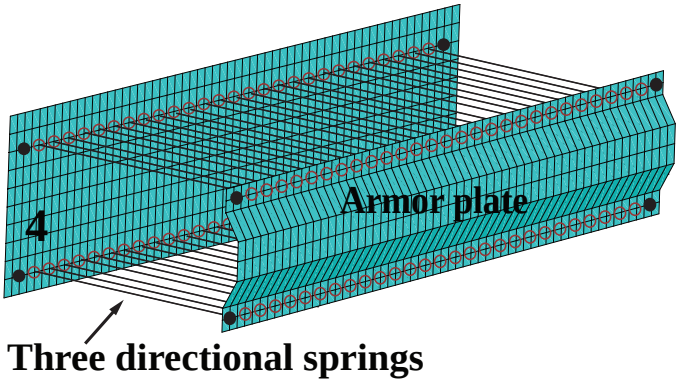

Figure 2: Springs modeling joints between substructure 4 and the armor plate

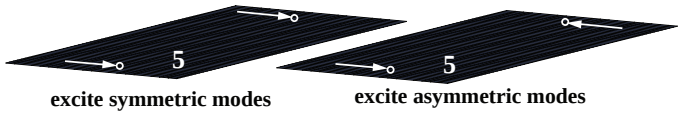

Figure 3: Dynamic loads applied to substructure 5 to excite symmetric and asymmetric modes of the entire structure

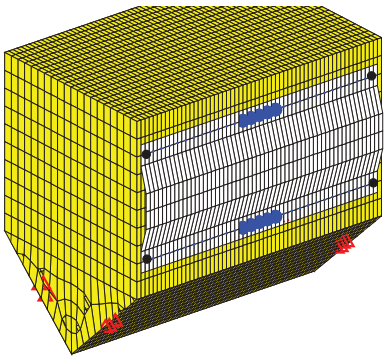

(a)

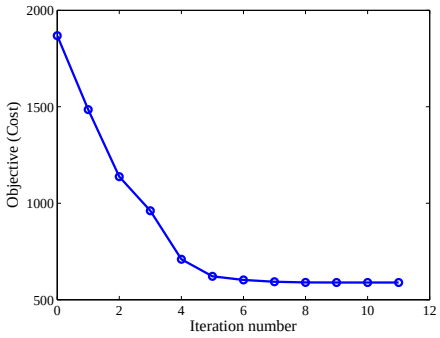

(b)

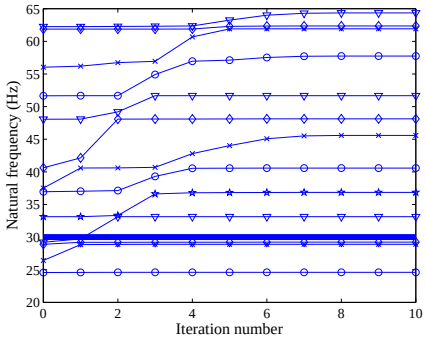

(c)

Figure 4: (a) 10 optimal joining locations, (b) convergence history, and (c) natural frequency variations for a 30 *Hz* excitation of the nominal structure

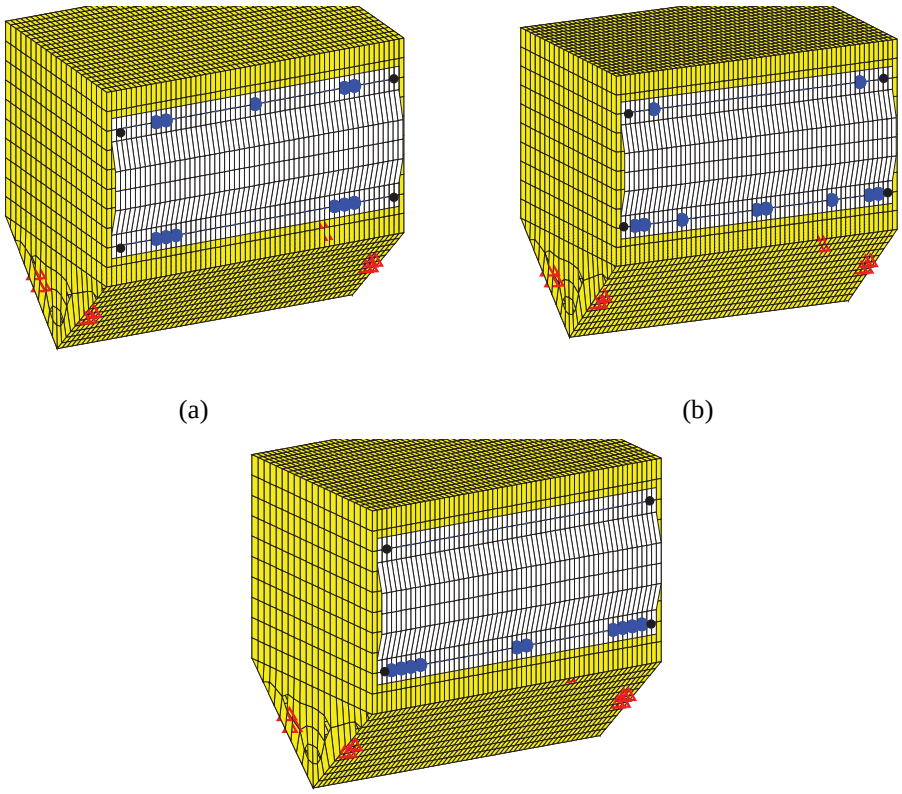

(a) (b)

(c)

Figure 5: Optimal joining locations for a 100 *Hz* excitation for (a) nominal structure, (b) case 1 (c) case 2 of thickness variation

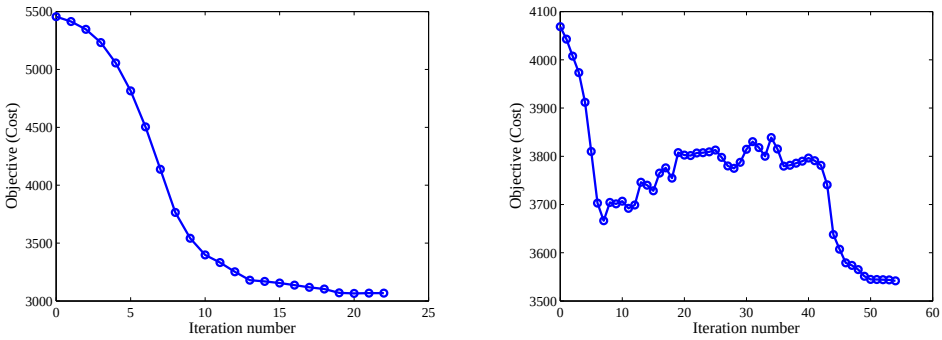

(a)

(b)

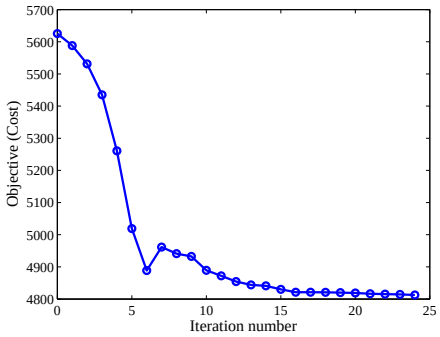

(c)

Figure 6: Convergence history for a 100 *Hz* excitation for (a) nominal structure, (b) case 1 (c) case 2 of thickness variation

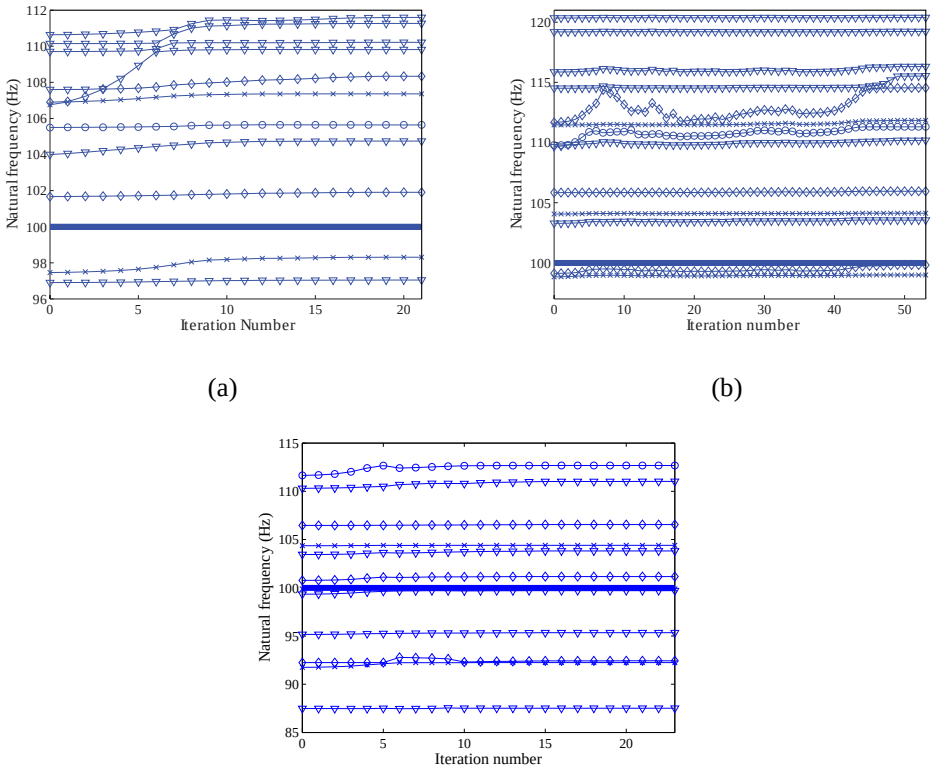

Figure 7: Natural frequency variation for a 100 *Hz* excitation for (a) nominal structure, (b) case 1 (c) case 2 of thickness variation